Letter

Atomic mass determination of uranium-238

Kathrin Kromer,[1,*] Chunhai Lyu,[1] Jacek Bieroń,[2] Menno Door,[1] Lucia Enzmann,[1,3] Pavel Filianin,[1] Gediminas Gaigalas,[4] Zoltán Harman,[1] Jost Herkenhoff,[1] Wenjia Huang,[5] Christoph H. Keitel,[1] Sergey Eliseev,[1] and Klaus Blaum[1]

[1]*Max-Planck-Institut für Kernphysik, 69117 Heidelberg, Germany*
[2]*Institute of Theoretical Physics, Jagiellonian University, 30-348 Kraków, Poland*
[3]*Ruprecht-Karls-Universität Heidelberg, 69117 Heidelberg, Germany*
[4]*Institute of Theoretical Physics and Astronomy, Vilnius University, 10222 Vilnius, Lithuania*
[5]*Advanced Energy Science and Technology Guangdong Laboratory, Huizhou 516007, China*

(Received 27 November 2023; accepted 8 January 2024; published 6 February 2024)

The atomic mass of uranium-238 has been determined to be 238.050 787 618(15) u, improving the literature uncertainty by two orders of magnitude. It is obtained from a measurement of the mass ratio of $^{238}U^{47+}$ and $^{132}Xe^{26+}$ ions with an uncertainty of 3.5×10^{-12}. The measurement was carried out with the Penning-trap mass spectrometer PENTATRAP and was accompanied by a calculation of the binding energies E_U and E_{Xe} of the 47 and 26 missing electrons of the two highly charged ions, respectively. These binding energies were determined using an *ab initio* multiconfiguration Dirac-Hartree-Fock method to be $E_U = 39\,927(10)$ eV and $E_{Xe} = 8\,971.2(21)$ eV. The new mass value will serve as a reference for high-precision mass measurements in the heavy mass region of the nuclear chart up to transuranium nuclides.

DOI: 10.1103/PhysRevC.109.L021301

Understanding the nuclear structure of heavy and superheavy elements provides clues about the mechanisms involved in synthesizing them and the reasons for their finite lifetimes [1,2]. Facilities measuring the masses of actinides and transactinides contribute to our understanding of the nuclear structure by examining binding energies and derivative values such as nucleon pairing strengths, two-nucleon separation energies, and shell gap parameters [3]. This experimental data benchmarks nuclear models which are essential for predicting properties of nuclides not accessible through experiments. It is imperative to test these models in regions where experimental data are becoming available, such as the region of the $N = 152$ subshell [4], to predict the next "doubly magic" nuclei after ^{208}Pb or the center and extent of the "island of stability" [5,6].

For high-precision mass measurements, Penning-trap mass spectrometry (PTMS) has nowadays become one of the leading methods of choice. PTMS now routinely achieves relative mass uncertainties in the range of 10^{-11} on stable or long-lived species [7–9] and in the range of 10^{-9} on radionuclides [10–12]. Ideally, carbon-12 is used as the reference mass, since the unified atomic mass unit u is defined as 1/12 of the mass of carbon-12 in its ground state. However, in reality it is often favorable to measure against a reference nuclide similar in mass to the nuclide of interest, so that many systematic uncertainties can be minimized. It is therefore desirable to have a network of nuclides with well-known masses that covers a wide mass range. The most precisely measured nuclides are sometimes referred to as the "mass backbone" [13,14]. This mass backbone and other known masses are evaluated in form of the Atomic Mass Evaluation (AME) [15], which considers all kinds of connections, from inertial to energy measurements.

The heavy mass region beyond uranium relies heavily on measurements relating them to the mass of a few uranium isotopes, whose masses are currently known to a precision of at best 5×10^{-9} [15]. In order to further research into nuclear structure, it is imperative to surpass this precision to benchmark advanced nuclear models. To overcome the limitation set by the reference, we have performed an ultraprecise mass measurement on uranium-238, thereby providing a significantly improved reference mass in the heavy mass region above lead, which contributes to the AME mass backbone.

In addition to serving as a reliable mass reference, an improved atomic mass value of uranium-238 is also needed for the planned investigation of the magnetic moment, and with it the g-factor of the bound-electron of hydrogenlike uranium at the experiment ALPHATRAP [16,17]. Electron g factors of heavy, highly charged ions provide stringent tests of bound-state quantum electrodynamics (QED) in strong fields as the size of the QED contribution to the g factor increases with the proton number Z [18]. However, the precision of a

*Corresponding author: kromer@mpi-hd.mpg.de

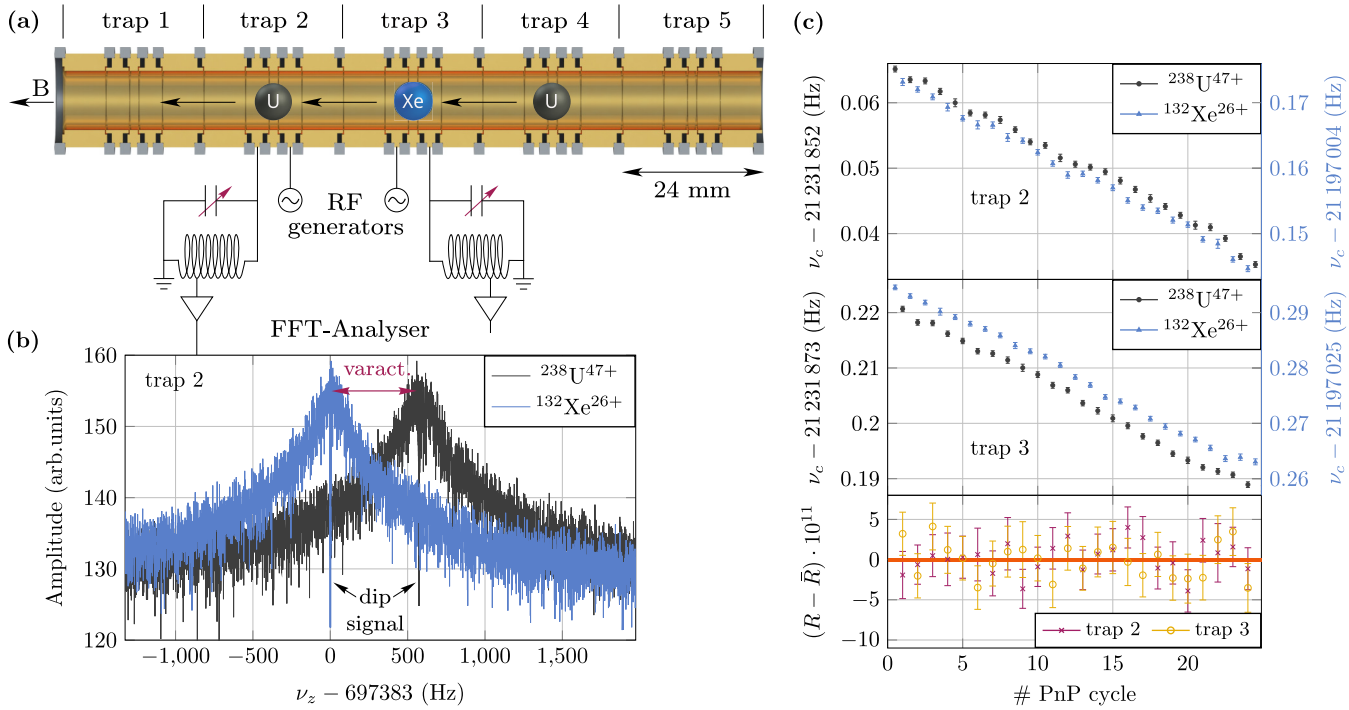

FIG. 1. (a) Sectional view of the Penning-trap tower with three ions in configuration 1. Configuration 2 is indicated by arrows. (b) Axial spectrum of trap 2 showing an overlay of a resonator with dip signal of the Xe ion and of the U ion at their respectively different resonator frequencies varied by the varactor. (c) Exemplary measurement run showing the determined cyclotron frequencies of both ions (y axis of the xenon ion is on the right in blue) and the ratios that can be formed by interpolation in time of the cyclotron frequencies (lower panel).

g-factor measurement is directly limited by the knowledge of the mass of the ion of interest. In order to achieve a determination of the electron g factor with a precision on the level of 10^{-9}, the mass of the ion has to be known to the same precision.

In this Letter, we will combine a Penning-trap mass ratio measurement and *ab initio* multiconfiguration Dirac-Hartree-Fock (MCDHF) binding-energy calculations to determine the atomic mass of uranium-238.

A determination of the mass of an ion m with charge q in a Penning trap is based on the measurement of the free cyclotron frequency $\nu_c = qB/(2\pi m)$ of the ion in a static homogeneous magnetic field B. In order to confine the particle's motion in all three dimensions, a Penning trap is composed of an electrostatic quadrupolar field in addition to the magnetic field. The combination of both fields forces the ion on a trajectory consisting of three independent eigenmotions (small to large in order of the size of the eigenfrequency): the magnetron motion with frequency ν_-, the axial motion with frequency ν_z, and the modified cyclotron motion with frequency ν_+. In order to obtain the free cyclotron frequency, the relation

$$\nu_c^2 = \nu_-^2 + \nu_z^2 + \nu_+^2 \tag{1}$$

can be used [19]. Since the magnetic field is not known precisely enough, one measures the cyclotron frequency of the ion of interest (subscripted ioi) with respect to the cyclotron frequency of a reference ion (subscripted ref) with well-known mass m_{ref} [15]. The measured ratio R of the cyclotron frequencies is just proportional to the ratio of the ions' masses, since the magnetic field cancels to first order:

$$R = \frac{\nu_{c,\mathrm{ioi}}}{\nu_{c,\mathrm{ref}}} = \frac{m_{\mathrm{ref}}}{m_{\mathrm{ioi}}} \frac{q_{\mathrm{ioi}}}{q_{\mathrm{ref}}}. \tag{2}$$

Usually, systematic effects increase with a larger mass difference, however, most systematic effects stemming from various trap imperfections and B-field inhomogeneities are minimized when using a similar charge-to-mass (q/m) ratio of the ion of interest and the reference ion. For this reason, mass measurements at PENTATRAP are carried out on a broad range of ion masses and charge states with the flexibility of choosing any reference ion that is most suited for each specific measurement [20,21]. For the determination of the absolute mass of uranium-238, the near q/m doublet $^{238}U^{47+}$ and $^{132}Xe^{26+}$ was chosen with a difference in q/m of $3.24 \times 10^{-4}\, e/\mathrm{u}$.

Highly charged ions are delivered to the mass spectrometer via a time-of-flight selective beamline [22] from a Heidelberg compact EBIT [23], equipped with a laser-desorption setup [24]. A small uranium laser target was used for the uranium ion production and a collimating gas-inlet system introduces xenon gas into the EBIT. The desired charge states of U and Xe were guided through the beamline by electrostatic lenses and a bender, time-of-flight selected by a pulsed operation of a Bradbury-Nielson gate [25] and slowed down by two pulsed drift tubes. For further information on the beamline, see [22]. Afterward, the slow ions can be captured inside the Penning trap tower made up of five individual traps. Two of the inner Penning traps are used for frequency measurements, and the other three are used for ion storage. There are in total three ions loaded in alternating sequence [see Fig. 1(a)]. This way,

the three ions can be moved up or down from configuration 1 to 2 between frequency determinations, effectively swapping the ion species in each of the measurement traps. On the one hand, this double measurement scheme allows for a doubling of measurement statistics since traps two and three are used in parallel to measure a cyclotron frequency ratio each. On the other hand, the two traps have different electric and magnetic field parameters, thus allowing for the cyclotron frequency ratio comparison to ensure a reliable evaluation of systematic shifts.

To determine the frequencies of the eigenmotions of the ions, cryogenic RLC resonators are connected to the axially offset electrodes in each measurement trap [see Fig. 1(a)]. The ion interacts with the resonator via the image current induced inside the trap electrodes by the axial motion of the ion. The ion's axial frequency can be brought into resonance with the center frequency of the resonator by tuning the trap depth. Once $\nu_z \approx \nu_{\mathrm{res}}$, the ion's axial motional amplitude will be damped to equilibrium with the thermal Johnson-Nyquist noise of the resonator, effectively cooling the ion's axial motion to around 4 K. Once the ion is cold, the resonator spectrum will show a "dip" signal at the ion's axial frequency [see Fig. 1(b)]. This nondestructive detection technique is called Fourier-transform ion-cyclotron resonance (FT-ICR) [26]. In order to determine the radial frequencies and reduce the radial amplitudes, one can couple each of them to the axial frequency, causing a "double-dip" from which the frequency of the coupled motion can be deduced [27]. The coupling drive can be induced by a frequency generator connected to a segmented, axially offset electrode.

In each trap, the potential is set to the same trap depth for both ion species, in order to minimize the potential systematic shifts of the measured cyclotron-frequency ratios due to the different ion positions in the traps. However, this results in different axial frequencies of the Xe and U ions due to their different q/m ratios. Variable GaAs capacitors (varactors) were recently implemented into the cryogenic RLC circuits of the traps [28] in order to adjust the resonance frequency of the detection circuit with respect to the axial frequency of the ions [see Figs. 1(a) and 1(b).

The largest of the three eigenfrequencies, the modified cyclotron frequency ν_+, is measured phase-sensitively using the pulse-and-phase (PnP) method [29]. A PnP sequence consists of an excitation pulse at the modified cyclotron frequency to set the initial phase, then a wait period called phase accumulation time t_{acc}, and finally a radiofrequency (rf) π pulse at the sideband frequency $\nu_{\mathrm{rf}} = \nu_+ - \nu_z$ to couple the modified cyclotron motion to the axial motion. The π pulse transfers not only the energy from the modified cyclotron motion to the axial motion but also its phase information, which can then be read out via the axial resonator, two amplification stages, a subsequent analog to digital converter, and by applying a Fourier transform. In order to subtract the starting phase and any shifts to the phase by the excitation and readout electronics, a "short" phase measurement with $t_{\mathrm{acc}} = 0.1$ s precedes the actual "long" measurement phase with an accumulation time of $t_{\mathrm{acc}} = 70$ to 100 s. To reduce the influence of electric field drifts in the trap, the axial frequency is measured during the long PnP phase measurement of the modified cyclotron frequency ν_+ via the dip technique. The magnetron frequency, being the smallest frequency, is only measured once in the beginning of every measurement run via the double dip method. The magnetron frequency of the reference ion is, however, calculated with the help of the magnetron frequency difference measurement, which was performed for the image charge shift measurement campaign (see Supplemental Material Sec. A [30]). The reason for using the calculated magnetron frequency instead of the measured absolute frequency is, that the cyclotron frequency ratio is more sensitive to the difference of the magnetron frequencies than the absolute frequencies. With measuring the difference instead of using the absolutely measured frequency for the reference ion, we avoid an unnecessarily large uncertainty of the magnetron frequency due to the double dip measurement. Figure 1(c) shows the cyclotron frequencies and ratios in both traps of a measurement run of ≈12 h. The ratios are formed by interpolating the cyclotron frequency of one ion to the point in time of the other ion's cyclotron frequency measurement. With the described measurement scheme, we were able to demonstrate determinations of relative mass ratios with uncertainties of a few 10^{-12} [31–33].

TABLE I. The systematic shifts and their uncertainties of the cyclotron frequency ratio determination. A shift ΔR is given as $\Delta R = \tilde{R} - R$ with R being the unperturbed frequency ratio and $\tilde{R}$ the measured value. The errors of the last three shifts are correlated due to their dependence on the uncertainty of the excitation radii. All values are given in 10^{-12}.

	Trap 2	Trap 3
ICS	−253.1(21)	−257.1(43)
Dip lineshape	0.0(11)	0.0(64)
Nonlinear phase	0.0(6)	0.00(22)
Relativistic	0.69(26)	0.5(6)
Electrost. anharm. C_4	0.00(23)	0.00(8)
Magnetic inhom. B_2	−0.042(12)	0.014(8)
Total systematic	−252.5(25)	−256.6(77)

The measured cyclotron frequency ratio $\tilde{R} = \nu_c(^{238}\mathrm{U}^{47+})/\nu_c(^{132}\mathrm{Xe}^{26+})$ is $\tilde{R}_2 = 1.001\,644\,000\,787\,9(30)$ and $\tilde{R}_3 = 1.001\,644\,000\,785\,5(25)$ for trap 2 and trap 3, respectively. This measured ratio was corrected for several systematic effects, see Table I, which are described in detail in the Supplemental Material [30]. The largest systematic correction comes from the image charge shift (ICS). This effect originates in the interaction between the ion and its image charge on the trap electrodes. The dip lineshape uncertainty originates from the fact that the analytical fit function of the dip spectrum [26] does not describe the spectrum comprehensively. In this case, the fit can yield an axial-frequency value shifted with respect to the true value. The nonlinear phase systematic is caused by a nonlinear transfer function of the ion's phase during the PnP phase readout. The uncertainty of the difference in motional radii between the uranium and the xenon ion, especially in the excited modified cyclotron motion, adds three correlated systematic effects, namely the relativistic

shift, the C_4, and the B_2 term. The relativistic effect describes the relativistic mass increase of the moving particles. The C_4 term approximates the effect that different motional radii have on the trap eigenfrequencies due to electrostatic anharmonicities, in leading order described by the coefficient C_4. Similarly, a quadratic inhomogeneity B_2 of the magnetic trapping field will also shift the frequencies of the two ions depending on their radii. With these corrections the cyclotron frequency ratios (with the statistical, systematic, and total error in first, second, and third bracket) were determined to be $R_2 = 1.001\,644\,001\,040\,4(30)(25)(38)$ and $R_3 = 1.001\,644\,001\,042\,1(25)(77)(81)$ for trap 2 and trap 3, respectively. The weighted average of the cyclotron frequency ratio is: $R = 1.001\,644\,001\,040\,7(35)$.

The absolute mass of uranium-238 can be determined via the following formula:

$$m(^{238}\mathrm{U}) = \frac{47}{26R} m(^{132}\mathrm{Xe}^{26+}) + 47m_e - E_\mathrm{U}/c^2$$
$$\text{with} \quad m(^{132}\mathrm{Xe}^{26+}) = m(^{132}\mathrm{Xe}) - 26m_e + E_\mathrm{Xe}/c^2. \qquad (3)$$

Here, R is the systematically corrected frequency ratio determined above, m_e signifies the mass of an electron [34], c is the speed of light, and $E_\mathrm{Xe} = 8\,971.2(21)$ eV is the binding-energy difference between Xe^{26+} and neutral Xe atom determined in our previous work [22,35]. The term $E_\mathrm{U} = 39.7(16)$ keV represents the binding-energy difference between U^{47+} and neutral U atom, with the 1.6-keV error bar mainly coming from the large uncertainties in the theoretical ionization potentials (IPs) listed in the NIST atomic database [36]. To improve the accuracy of E_U, in this work, we will calculate it via the *ab initio* fully relativistic MCDHF and relativistic configuration interaction (RCI) methods [37–39] implemented in the GRASP2018 code [40–42]. For the sake of computational efficiency, we perform a full calculation for the binding-energy difference $E_\mathrm{U}^{6\text{–}46}$ between U^{46+} and U^{6+} ions that bear closed-shell ground states, with the IPs of the outermost six electrons and the IP of U^{46+} being treated separately.

In the calculation, the atomic state functions (ASFs) are expanded as linear combinations of configuration state functions (CSFs), which are jj-coupled Slater determinants of one-electron orbitals, with appropriate angular symmetry and parity. We first solve the MCDHF equations self-consistently [37–39] to optimize the radial wave functions of the one-electron orbital under the Dirac-Coulomb Hamiltonian. Then, the RCI method is employed to calculate the contributions from frequency-dependent and frequency-independent transverse photon interactions, the mass shift, and QED effects. Different from previous calculations for Pb^{4+}, where the intermediately charged ion Pb^{22+} had been used to bridge the calculations of the correlation energy of the 78 electrons, in this work, we have modified the GRASP2018 code such that we can directly account for the full single and double (SD) electron exchange correlations of the 86 electrons in U^{6+}. The results are summarized in Table IV of the Supplemental Materials [30]. We find that the term $E_\mathrm{U}^{6\text{–}46}$ is dominated by the single-configuration Dirac-Hartree-Fock binding-energy difference. Such single-configuration calculations give rise to a value of 37 110.01(8) eV with a contribution of $-0.47(1)$, $-0.02(1)$, and $-0.65(6)$ eV from the finite nuclear size, the mass shift, and the QED effects, respectively. The Breit interaction and the frequency-dependent transverse-photon interaction together contribute -16.26 eV whose uncertainty will be examined later in the correlation energies. To account for the correlation effects, we systematically expand the size of the CSF basis set by allowing SD excitation of electrons from all the occupied orbitals to the systematically increasing set of correlation orbitals. These correlation orbitals are added and optimized with the layer-by-layer approach [41] up to $n = 11$ (n is the principal quantum number), where all orbitals with orbital angular momentum from 0 up to $n-1$ are included. By extrapolating to $n = \infty$ [35] we obtain a contribution of 64.7(17) eV to $E_\mathrm{U}^{6\text{–}46}$. The contribution from correlation effects beyond the SD electron excitations are conservatively constrained to be of 6.3(63) eV [22,35]. Finally, we arrive at $E_\mathrm{U}^{6\text{–}46} = 37\,164(8)$ eV, with the uncertainty being dominated by higher-order correlation effects (see Supplemental Material Sec. E for more details [30]).

To derive E_U, one has to add up the IP of U^{46+} as well as the IPs of the outermost 6 electrons of the uranium atom. For the IP of U^{46+}, it is calculated to be 2580.9(1) eV based on CSF basis set generated via SD excitations from the $4s$ orbital. For low charged uranium, the first three IPs are known experimentally [36]. There is also an experimental value for the IP of U^{3+}, but it is around 4 eV larger than that from a recent theoretical calculation based on the multireference configuration interaction method [43]. Nevertheless, our calculations are in good agreement with the values presented in Ref. [43]: with CSFs generated via SD excitation of electrons starting from the $6s$ orbital, we arrive at values of 33.12(42), 48.14(42) and 63.15(42) eV for the IPs of U^{3+}, U^{4+}, and U^{5+}, respectively. In total, we obtain $E_\mathrm{U}^{0\text{–}6} = 182.0(20)$ eV for the total binding energy of the outermost six electrons. Thus, the binding-energy difference between neutral uranium and U^{47+} is calculated to be $E_\mathrm{U} = 39\,927(10)$ eV which is more than two orders of magnitude more accurate than the NIST value [36].

By combining the measured cyclotron frequency ratio with the calculated electron binding energies and the literature xenon-132 mass [15], the atomic mass of uranium-238 was calculated using Eq. (3) which yields the final value of $m(^{238}\mathrm{U}) = 238.050\,787\,618(15)$ u. This value represents an improvement of two orders of magnitude compared to the current literature value of $m(^{238}\mathrm{U}) = 238.050\,786\,9(16)$ u [15]. The associated mass excess is correspondingly determined to be 47 308.367(14) keV. With the reduced mass uncertainty of uranium-238, the atomic mass of uranium-239 which is connected to the 238 mass via a neutron capture process and plutonium-242 connected via a well-known α decay energy will be improved as well by a factor of 9 and 1.5, respectively [15]. The mass excess of ^{239}U is readjusted to be 50 573.31(17) keV and the one of ^{242}Pu is 54 717.3(8) keV.

With the new relative mass precision of 6×10^{-11} achieved in this work, heavy mass determinations on short-lived nuclei, using the uranium mass as a reference, will not be limited by reference precision for the foreseeable future. A future g-factor determination of the bound electron of $^{238}U^{91+}$ for

tests of bound-state quantum electrodynamics can now be carried out with the same precision as that of the mass [17].

This work comprises parts of the Ph.D. thesis work of K.K. to be submitted to Heidelberg University, Germany. This work is part of and funded by the Max-Planck-Gesellschaft and the DFG (German Research Foundation) - Project-ID No. 273811115 - SFB 1225 ISOQUANT. The project received funding from the European Research Council (ERC) under the European Union's Horizon 2020 research and innovation programme under Grant Agreement No. 832848 - FunI. Furthermore, we acknowledge funding and support by the International Max-Planck Research School for Precision Tests of Fundamental Symmetries and the Max Planck, RIKEN, PTB Center for Time, Constants and Fundamental Symmetries.

[1] A. Sobiczewski and K. Pomorski, Description of structure and properties of superheavy nuclei, Prog. Part. Nucl. Phys. **58**, 292 (2007).

[2] J. Hamilton, S. Hofmann, and Y. Oganessian, Search for superheavy nuclei, Annu. Rev. Nucl. Part. Sci. **63**, 383 (2013).

[3] G. Audi, The Evaluation of Atomic Masses, in *Atomic Physics at Accelerators: Mass Spectrometry*, edited by D. Lunney, G. Audi, and H.-J. Kluge (Springer Netherlands, Dordrecht, 2001), pp. 7–34.

[4] M. Block, F. Giacoppo, F.-P. Heßberger, and S. Raeder, Recent progress in experiments on the heaviest nuclides at SHIP, Riv. Nuovo Cim. **45**, 279 (2022).

[5] A. Poves and F. Nowacki, The Nuclear Shell Model, in *An Advanced Course in Modern Nuclear Physics*, edited by J. M. Arias and M. Lozano, Lecture Notes in Physics (Springer, Berlin, Heidelberg, 2001), pp. 70–101.

[6] S. A. Giuliani, Z. Matheson, W. Nazarewicz, E. Olsen, P.-G. Reinhard, J. Sadhukhan, B. Schuetrumpf, N. Schunck, and P. Schwerdtfeger, Colloquium: Superheavy elements: Oganesson and beyond, Rev. Mod. Phys. **91**, 011001 (2019).

[7] D. J. Fink and E. G. Myers, Deuteron-to-proton mass ratio from the cyclotron frequency ratio of H_2^+ to D^+ with H_2^+ in a resolved vibrational state, Phys. Rev. Lett. **124**, 013001 (2020).

[8] S. Sasidharan, O. Bezrodnova, S. Rau, W. Quint, S. Sturm, and K. Blaum, Penning-trap mass measurement of helium-4, Phys. Rev. Lett. **131**, 093201 (2023).

[9] P. Filianin, C. Lyu, M. Door, K. Blaum, W. J. Huang, M. Haverkort, P. Indelicato, C. H. Keitel, K. Kromer, D. Lange, Y. N. Novikov, A. Rischka, R. X. Schüssler, C. Schweiger, S. Sturm, S. Ulmer, Z. Harman, and S. Eliseev, Direct Q-value determination of the β^- decay of ^{187}Re, Phys. Rev. Lett. **127**, 072502 (2021).

[10] M. Dworschak, M. Block, D. Ackermann, G. Audi, K. Blaum, C. Droese, S. Eliseev, T. Fleckenstein, E. Haettner, F. Herfurth, F. P. Heßberger, S. Hofmann, J. Ketelaer, J. Ketter, H.-J. Kluge, G. Marx, M. Mazzocco, Yu. N. Novikov, W. R. Plaß, A. Popeko *et al.*, Penning trap mass measurements on nobelium isotopes, Phys. Rev. C **81**, 064312 (2010).

[11] M. Hukkanen, W. Ryssens, P. Ascher, M. Bender, T. Eronen, S. Grévy, A. Kankainen, M. Stryjczyk, L. Al Ayoubi, S. Ayet, O. Beliuskina, C. Delafosse, W. Gins, M. Gerbaux, A. Husson, A. Jokinen, D. A. Nesterenko, I. Pohjalainen, M. Reponen, S. Rinta-Antila *et al.*, Odd-odd neutron-rich rhodium isotopes studied with the double Penning trap JYFLTRAP, Phys. Rev. C **107**, 014306 (2023).

[12] J. Karthein, D. Atanasov, K. Blaum, S. Eliseev, P. Filianin, D. Lunney, V. Manea, M. Mougeot, D. Neidherr, Y. Novikov, L. Schweikhard, A. Welker, F. Wienholtz, and K. Zuber, Direct decay-energy measurement as a route to the neutrino mass, Hyperfine Interact **240**, 61 (2019).

[13] G. Audi, M. Wang, A. H. Wapstra, F. G. Kondev, M. MacCormick, and B. Pfeiffer, The AME2012 atomic mass evaluation, Chin. Phys. C **36**, 1287 (2012).

[14] C. Guénaut, G. Audi, D. Beck, K. Blaum, G. Bollen, P. Delahaye, F. Herfurth, A. Kellerbauer, H. J. Kluge, D. Lunney, S. Schwarz, L. Schweikhard, and C. Yazidjian, Extending the mass "backbone" to short-lived nuclides with ISOLTRAP, Eur. Phys. J. A **25**, 35 (2005).

[15] M. Wang, W. J. Huang, F. G. Kondev, G. Audi, and S. Naimi, The AME 2020 atomic mass evaluation (II). Tables, graphs and references, Chin. Phys. C **45**, 030003 (2021).

[16] S. Sturm, I. Arapoglou, A. Egl, M. Höcker, S. Kraemer, T. Sailer, B. Tu, A. Weigel, R. Wolf, J. C. López-Urrutia, and K. Blaum, The ALPHATRAP experiment, Eur. Phys. J. Spec. Top. **227**, 1425 (2019).

[17] J. Morgner, B. Tu, C. M. König, T. Sailer, F. Heiße, H. Bekker, B. Sikora, C. Lyu, V. A. Yerokhin, Z. Harman, J. R. Crespo López-Urrutia, C. H. Keitel, S. Sturm, and K. Blaum, Stringent test of QED with hydrogen-like tin, Nature (London) **622**, 53 (2023).

[18] T. Beier, The g_j factor of a bound electron and the hyperfine structure splitting in hydrogenlike ions, Phys. Rep. **339**, 79 (2000).

[19] L. S. Brown and G. Gabrielse, Precision spectroscopy of a charged particle in an imperfect Penning trap, Phys. Rev. A **25**, 2423 (1982).

[20] J. Repp, C. Böhm, J. R. Crespo López-Urrutia, A. Dörr, S. Eliseev, S. George, M. Goncharov, Y. N. Novikov, C. Roux, S. Sturm, S. Ulmer, and K. Blaum, PENTATRAP: A novel cryogenic multi-Penning-trap experiment for high-precision mass measurements on highly charged ions, Appl. Phys. B **107**, 983 (2012).

[21] C. Roux, C. Böhm, A. Dörr, S. Eliseev, S. George, M. Goncharov, Y. N. Novikov, J. Repp, S. Sturm, S. Ulmer, and K. Blaum, The trap design of PENTATRAP, Appl. Phys. B **107**, 997 (2012).

[22] K. Kromer, C. Lyu, M. Door, P. Filianin, Z. Harman, J. Herkenhoff, W. Huang, C. H. Keitel, D. Lange, Y. N. Novikov, C. Schweiger, S. Eliseev, and K. Blaum, High-precision mass measurement of doubly magic ^{208}Pb, Eur. Phys. J. A **58**, 202 (2022).

[23] P. Micke, S. Kühn, L. Buchauer, J. R. Harries, T. M. Bücking, K. Blaum, A. Cieluch, A. Egl, D. Hollain, S. Kraemer, T. Pfeifer, P. O. Schmidt, R. X. Schüssler, Ch. Schweiger, T. Stöhlker, S. Sturm, R. N. Wolf, S. Bernitt, and J. R. Crespo López-Urrutia, The Heidelberg compact electron beam ion traps, Rev. Sci. Instrum. **89**, 063109 (2018).

[24] Ch. Schweiger, C. M. König, J. R. Crespo López-Urrutia, M. Door, H. Dorrer, Ch. E. Düllmann, S. Eliseev, P. Filianin, W. Huang, K. Kromer, P. Micke, M. Müller, D. Renisch, A.

Rischka, R. X. Schüssler, and K. Blaum, Production of highly charged ions of rare species by laser-induced desorption inside an electron beam ion trap, Rev. Sci. Instrum. **90**, 123201 (2019).
[25] N. E. Bradbury and R. A. Nielsen, Absolute values of the electron mobility in hydrogen, Phys. Rev. **49**, 388 (1936).
[26] X. Feng, M. Charlton, M. Holzscheiter, R. A. Lewis, and Y. Yamazaki, Tank circuit model applied to particles in a Penning trap, J. Appl. Phys. **79**, 8 (1996).
[27] E. A. Cornell, R. M. Weisskoff, K. R. Boyce, and D. E. Pritchard, Mode coupling in a Penning trap: π pulses and a classical avoided crossing, Phys. Rev. A **41**, 312 (1990).
[28] F. Heiße, F. Köhler-Langes, S. Rau, J. Hou, S. Junck, A. Kracke, A. Mooser, W. Quint, S. Ulmer, G. Werth, K. Blaum, and S. Sturm, High-precision measurement of the proton's atomic mass, Phys. Rev. Lett. **119**, 033001 (2017).
[29] E. A. Cornell, R. M. Weisskoff, K. R. Boyce, R. W. Flanagan, G. P. Lafyatis, and D. E. Pritchard, Single-ion cyclotron resonance measurement of $M(CO^+)/M(N_2^+)$, Phys. Rev. Lett. **63**, 1674 (1989).
[30] See Supplemental Material at http://link.aps.org/supplemental/10.1103/PhysRevC.109.L021301 for details on the systematic uncertainties and on the theoretical binding energy calculations.
[31] K. Kromer, C. Lyu, M. Door, P. Filianin, Z. Harman, J. Herkenhoff, P. Indelicato, C. H. Keitel, D. Lange, Y. N. Novikov, C. Schweiger, S. Eliseev, and K. Blaum, Observation of a low-lying metastable electronic state in highly charged lead by Penning-trap mass spectrometry, Phys. Rev. Lett. **131**, 223002 (2023).
[32] C. Schweiger, M. Braß, V. Debierre, M. Door, H. Dorrer, C. E. Düllmann, C. Enss, P. Filianin, L. Gastaldo, Z. Harman *et al.*, Direct high-precision Penning-trap measurement of the Q-value of the electron capture in ^{163}Ho for the determination of the electron neutrino mass, Nat. Phys. (to be published).
[33] F. Heiße, M. Door, T. Sailer, P. Filianin, J. Herkenhoff, C. König, K. Kromer, D. Lange, J. Morgner, A. Rischka, C. Schweiger, B. Tu, Y. Novikov, S. Eliseev, S. Sturm, and K. Blaum, High-precision determination of g actors and masses of $^{20}Ne^{9+}$ and $^{22}Ne^{9+}$, Phys. Rev. Lett. **131**, 253002 (2023).
[34] J. Zatorski, B. Sikora, S. G. Karshenboim, S. Sturm, F. Köhler-Langes, K. Blaum, C. H. Keitel, and Z. Harman, Extraction of the electron mass from g-factor measurements on light hydrogenlike ions, Phys. Rev. A **96**, 012502 (2017).
[35] C. Lyu, B. Sikora, Z. Harman, and C. H. Keitel, Extreme field calculations for Penning ion traps and corresponding strong laser field scenarios, Mol. Phys. e2252105 (2023).
[36] A. Kramida, Yu. Ralchenko, J. Reader, and NIST ASD Team, NIST Atomic Spectra Database (version 5.8), [Online], https://physics.nist.gov/asd (National Institute of Standards and Technology, Gaithersburg, MD, 2021).
[37] I. P. Grant, Relativistic calculation of atomic structures, Adv. Phys. **19**, 747 (1970).
[38] J. P. Desclaux, D. F. Mayers, and F. O'Brien, Relativistic atomic wave functions, J. Phys. B **4**, 631 (1971).
[39] I. P. Grant, *Relativistic Quantum Theory of Atoms and Molecules*, Springer Series on Atomic, Optical, and Plasma Physics, Vol. 40 (Springer, Berlin, 2007).
[40] C. Froese Fischer, G. Gaigalas, P. Jönsson, and J. Bieroń, GRASP2018—A FORTRAN 95 version of the General Relativistic Atomic Structure Package, Comput. Phys. Commun. **237**, 184 (2019).
[41] P. Jönsson, G. Gaigalas, C. Froese Fischer, J. Bieroń, I. P. Grant, T. Brage, J. Ekman, M. Godefroid, J. Grumer, J. Li, and W. Li, GRASP manual for users, Atoms **11**, 68 (2023).
[42] P. Jönsson, M. Godefroid, G. Gaigalas, J. Ekman, J. Grumer, W. Li, J. Li, T. Brage, I. P. Grant, J. Bieroń, and C. Froese Fischer, An introduction to relativistic theory as implemented in GRASP, Atoms **11**, 7 (2023).
[43] D. H. Bross, P. Parmar, and K. A. Peterson, Multireference configuration interaction calculations of the first six ionization potentials of the uranium atom, J. Chem. Phys. **143**, 184308 (2015).